THE ASTROPHYSICAL JOURNAL, 536:406–415, 2000 June 10


# INFALL SIGNATURES IN SPECTRAL LINE PROFILES OF PROTOSTELLAR ENVELOPES

HIROHIKO MASUNAGA[1] AND SHU-ICHIRO INUTSUKA[2]
Division of Theoretical Astrophysics, National Astronomical Observatory, Mitaka, Tokyo 181-8588, Japan
*Received 1999 April 19; accepted 2000 January 20*

## ABSTRACT

A double-peaked profile with a stronger blue peak in a molecular line spectrum is considered strong evidence for the infall motion in the gas envelope surrounding a protostar. Some past studies performed model calculations for reproducing observed spectral profiles using simplified dynamical models such as isothermal similarity solutions. However, validity of the similarity solutions for spectral line synthesis should be examined in comparison with more realistic dynamical models.

In this paper we carry out theoretical modeling of molecular line spectra, adopting a spherically symmetric radiation hydrodynamical model for protostar formation taken from a recent work by the authors. This study concentrates on how infall motions could account for the asymmetric line profiles observed toward protostellar sources. We do not explicitly consider the effects of rotation and outflows on the generation of line profiles. In our numerical code for the non-LTE line transfer, the level populations are fully consistent with the radiation field under an arbitrary physical structure in spherical symmetry, and hence, reliable spectral synthesis has been enabled and compared to the LTE, large velocity gradient (or Sobolev), and microturbulence approximations.

Contrary to the remarks by Zhou, we do not find an overestimation of line widths, although the dynamical evolution resembles the Larson-Penston solution rather than the expansion-wave solution. Furthermore, the infall motion produces wings extending to $v = \pm 2$ km s$^{-1}$ in line spectra, in contrast to previous works where wings could not be produced by infall models. These results imply that simplified infall models, such as the isothermal similarity solutions adopted by previous authors, are not always suitable to the detailed modeling of line spectra.

*Subject headings:* hydrodynamics — ISM: clouds — ISM: molecules — line: profiles — radiative transfer — stars: formation

## 1. INTRODUCTION

Observations have revealed that protostellar cloud cores often show characteristic profiles in molecular line spectra. In particular, a double-peaked profile with a blue asymmetry in an optically thick line is often observed, which is considered strong evidence for infall motion. The original idea is traced back to Snell & Loren (1977) and Leung & Brown (1977). Walker et al. (1986) provided spectroscopic evidence for infall motions around a cold *IRAS* source in Ophiuchus through a line profile analysis and proposed that the object is a young protostar under dynamical growth. Zhou (1992) systematically investigated line features as evidence of infall motions using the isothermal self-similar collapse solutions. Detailed modeling of line profiles for B335 was done, and a double-peaked spectrum with a stronger blue peak was confirmed to be a good qualitative signature of infall (Choi et al. 1995). Recently, some statistical investigations were done for protostellar candidates including class 0 and class I sources (Gregersen et al. 1997; Mardones et al. 1997). Mardones et al. (1997) revealed that line profiles in class 0 sources are statistically more skewed toward the blueshifted velocity than in class I sources, which implies that line asymmetry is a good indicator of the evolutionary status at early stages of star formation. On the other hand, some previous models for infall motions do not account for a wing component (e.g., Gregersen et al. 1997), and hence spectral profiles of individual sources are not always modeled successfully. A wing component can be attributed to outflows, as is usually done, but no theoretical models are available to fit observations including the contamination of outflows.

In order to reproduce the observed line profiles, previous workers typically adopted the isothermal similarity solutions, which consist of a family of solutions including two well-known representatives, i.e., the "LP model" and the "Shu model" according to the definition by Zhou (1992). The LP model contains, in addition to the original solution derived by Larson (1969) and Penston (1969) for $t < 0$, the continuous counterpart obtained by Hunter (1977) after $t$ exceeds zero. Here $t = 0$ denotes the instance when the central density diverges to infinity, or when the central star is supposed to be born. On the other hand, the Shu model contains a sequence of the hydrostatic equilibrium solutions for $t < 0$ and the expansion-wave collapse solution (Shu 1977) for $t > 0$. Zhou (1992) calculated emergent line spectra for these two models, and he reached the conclusion that the LP model overestimates the velocity width of CS lines in comparison with observations.

This seems, however, to arise from an unrealistic condition in the "naive" LP model, where the infall velocity increases with radius and converges to a finite value ($= 3.26 c_s$) at infinity. On the other hand, numerical experiments by radiation hydrodynamic (RHD) calculations (Larson 1969; Masunaga, Miyama, & Inutsuka 1998) have found that the initial phase of protostellar evolution is excellently approximated by the LP model under reasonable boundary conditions supposing a fixed boundary or a constant external pressure at a finite radius. This "realistic" LP model has decreasing infalling velocity at a large radius,

[1] Present address: Earth Observation Research Center, 1-9-9 Roppongi, Minato-ku, Tokyo 106-0032, Japan; masunaga@eorc.nasda.go.jp.
[2] inutsuka@th.nao.ac.jp.

and hence it would provide a different spectral profile from that obtained by Zhou (1992). The expansion-wave collapse solution is believed to provide a more reasonable model, but it is still too idealized for detailed spectral synthesis. The applicability of the isothermal similarity solutions remains unexamined, and thus a more detailed study on spectral line profiles is necessary using an elaborate theoretical model.

In this paper we adopt a theoretical model by Masunaga (1999) and Masunaga & Inutsuka (2000), where RHD calculations were performed in spherical symmetry to establish a realistic model for protostar formation. In addition, we have developed a numerical code for non-LTE spectral line synthesis where the level populations are determined fully consistently with the radiation field under arbitrary physical structures in spherical symmetry. Our numerical scheme, therefore, enables us to yield more reliable results than the LTE, large velocity gradient (LVG; or Sobolev), and microturbulence approximations, where some simplifications on the level populations or velocity structure are imposed. Since our collapse model assumes spherical symmetry, this study concentrates on to what extent the infall motions account for the asymmetric line profiles apart from the effects of rotation and outflows.

## 2. NUMERICAL SCHEME

We introduce our numerical scheme for spectral line synthesis in this section.

### 2.1. *Basic Equations*

The radiative transfer equation is solved under the given absorption coefficient, $\alpha_\nu$, and the source function, $S_\nu$:

$$\mu \frac{\partial I_{\mu\nu}}{\partial r} + \frac{1-\mu^2}{r} \frac{\partial I_{\mu\nu}}{\partial \mu} = -\alpha_\nu (I_{\mu\nu} - S_\nu) , \tag{1}$$

where

$$\alpha_\nu = \frac{h\nu}{4\pi} \varphi_{J+1,J}(\mu, \nu)(n_J B_{J,J+1} - n_{J+1} B_{J+1,J}) , \tag{2}$$

$$S_\nu = \frac{n_{J+1} A_{J+1,J}}{(n_J B_{J,J+1} - n_{J+1} B_{J+1,J})} . \tag{3}$$

Here $\mu$ is direction cosine. The Einstein coefficients for the dipole radiation emitted by rotational transitions between the quantum numbers of $J$ and $J+1$ are

$$B_{J+1,J} = \frac{32\pi^4 \mu_d^2}{3h^2 c} \frac{J+1}{2J+3} ,$$

$$B_{J,J+1} = \frac{2J+3}{2J+1} B_{J+1,J} ,$$

$$A_{J+1,J} = \frac{16hB^3}{c^2} (J+1)^3 B_{J+1,J} ,$$

where $\mu_d$ is the electric dipole moment and $B$ is the rotation constant. Only the transitions between $\Delta J = \pm 1$ are permitted for the dipole radiation. The rotation constant is defined by

$$B \equiv \frac{h}{8\pi^2 I} ,$$

where $I$ is the moment of inertia of a molecule. The energy level corresponding to the $J$th angular momentum $L_J = [J(J+1)]^{1/2}\hbar$ is given by

$$E_J = BJ(J+1)h .$$

Here we consider only linear molecules.

In order to evaluate $\alpha_\nu$ and $S_\nu$, population at every energy level is solved.

$$\begin{aligned} \frac{\partial n_J}{\partial t} = {} & n_{J+1}(A_{J+1,J} + \bar{J}_{J+1,J} B_{J+1,J}) \\ & + n_{J-1} \bar{J}_{J,J-1} B_{J-1,J} \\ & - n_J (A_{J,J-1} + \bar{J}_{J,J-1} B_{J,J-1}) \\ & - n_J \bar{J}_{J+1,J} B_{J,J+1} \\ & + N_{\mathrm{H_2}} \left( \sum_{J'} \gamma^c_{J',J} n_{J'} - n_J \sum_{J'} \gamma^c_{J,J'} \right) , \end{aligned} \tag{4}$$

where

$$\bar{J}_{J+1,J} = \tfrac{1}{2} \int_{-1}^{1} d\mu \int_0^\infty d\nu I_{\mu\nu} \varphi_{J+1,J}(\mu, \nu) \tag{5}$$

and $\gamma^c_{J',J}$ is the collisional transition rate of $J' \to J$. In our calculations the left-hand side of equation (4) is set to be zero (i.e., $\partial/\partial t \equiv 0$).

The line profile function for static media, $\varphi^0_{J+1,J}(\nu)$, is assumed here to be the thermal Doppler broadening:

$$\varphi^0_{J+1,J}(\nu) = \frac{1}{\Delta\nu_D \sqrt{\pi}} \exp\left[ -\left( \frac{\nu - \nu_{J+1,J}}{\Delta\nu_D} \right)^2 \right] , \tag{6}$$

where

$$\Delta\nu_D = \frac{\nu_{J+1,J}}{c} \sqrt{\frac{2kT}{m}} .$$

The profile function is shifted in the frequency space as a result of the bulk motion with radial velocity $v_r$;

$$\varphi_{J+1,J}(\mu, \nu) = \varphi^0_{J+1,J}\left( \nu - \frac{\nu_{J+1,J}}{c} v_r \mu \right) . \tag{7}$$

### 2.2. *Computational Procedure*

The computational procedure follows a typical $\Lambda$-iteration method. First, the transfer equation (1) is integrated under trial values for $n_J$ in equations (2) and (3). The Boltzmann distribution is used as trial level populations. Second, equation (4) is solved by using $\bar{J}_{J+1,J}$, which is estimated by the solution of the transfer equation. Newly obtained $n_J$ provides improved values of the absorption coefficient and source function, with which equation (1) is solved again. The above procedure is iterated until the self-consistent solution between the source function and the radiation field is obtained everywhere in the collapsing cloud. The criterion for convergence is that the maximum of relative errors in $\alpha_\nu$ and $S_\nu$ is below 1%.

Together with the radiative transfer equations for $N$ transitions from $J = 0$ to $N$, equation (4) is solved for each $J$ between 0 and $N-1$ along with the normalization equation,

$$\sum_{J=0}^{N} n_J = \alpha_c X n_{\mathrm{H_2}} , \tag{8}$$

where $X$ is the fractional abundance of the molecular tracer relative to molecular hydrogen. A dimensionless factor $\alpha_c$ is unity when most molecules occupy rotational levels lower than $J = N$. Otherwise, $\alpha_c$ should be adjusted appropriately to give the correct normalization. Correction by $\alpha_c$ becomes important when $T$ is large enough to pump up the populations to higher levels than $J = N$. In our cases such hot regions are confined near the central protostar, where the density is so high that the Boltzmann distribution is achieved and LTE can be assumed. We therefore determine $\alpha_c$ assuming that $n_J$ obeys the Boltzmann distribution:

$$\alpha_c = \sum_{J=0}^{N} (2J+1) \exp\left(-\frac{E_J}{kT}\right) \Big/ \sum_{J=0}^{\infty} (2J+1) \exp\left(-\frac{E_J}{kT}\right). \tag{9}$$

Emergent spectra obtained from the converged solutions are presented in terms of the antenna temperature, $T_A$, versus the Doppler velocity. The antenna temperature is

$$T_A = \frac{\int_{\text{source}} T_B(\Omega) P_\nu(\Omega) d\Omega}{\int_{4\pi} P_\nu(\Omega) d\Omega}, \tag{10}$$

where $P_\nu$ represents a Gaussian beam pattern with a given FWHM, which is given as the wavelength divided by the diameter of an imaginary telescope. The brightness temperature, $T_B$, is obtained by

$$T_B = \frac{c^2}{2\nu^2 k} I_\nu, \tag{11}$$

where $I_\nu$ is the calculated spectral profile. Our numerical code permits an off-center beam convolution in addition to the centered beam. The aperture efficiency and the beam efficiency of the telescope are assumed to be unity (100%) in our calculations.

The Doppler velocity is simply defined by

$$\frac{v}{c} = \frac{f - f_0}{f_0}, \tag{12}$$

where $c$ is the speed of light, $f$ is the frequency, and $f_0$ is the frequency at the line center measured in the rest frame.

## 3. CALCULATIONS AND RESULTS

### 3.1. *Molecular Tracers*

We use CS, $HCO^+$, and $H^{13}CO^+$ as molecular tracers for collapsing clouds. Rotational transitions of these molecules have high critical densities, $\gtrsim 10^5$–$10^6$ cm$^{-3}$ in $n_{H_2}$, at which the collisional deexcitation rate is balanced with Einstein's $A$-coefficient. They therefore trace dense regions in molecular clouds, which are candidates for star-forming cloud cores. Typical abundances are $10^{-9}$–$10^{-8}$ relative to molecular hydrogen for CS and $HCO^+$ and smaller by nearly 1/100 for $H^{13}CO^+$. For probable values of column density of star-forming cores, $HCO^+$ lines are typically opaque in contrast to $H^{13}CO^+$ lines, which are optically thin because of their low abundance. Molecules are assumed to be destroyed for $T > 2000$ K. Spectral profiles do not suffer from the arbitrariness of the destruction temperature since the region where molecules are destroyed occupies only a negligible volume in the cloud core.

Tables 1 and 2 show the parameters used in calculations for the molecular tracers. The collisional deexcitation rates, $\gamma^c_{J',J}(J' > J)$, are taken from tabulated data by Green & Chapman (1978) for CS and from data by Monteiro (1985; for $J = 0$ to $J = 3$) and Green (1975; for $J = 4$ and $J = 5$) for $HCO^+$ and $H^{13}CO^+$, scaled appropriately. The collisional excitation rate, $\gamma^c_{J,J'}(J' > J)$, is calculated using $\gamma^c_{J',J}$ from detailed balance:

$$\frac{\gamma^c_{J,J'}}{\gamma^c_{J',J}} = \frac{2J'+1}{2J+1} \exp\left(-\frac{E_{J',J}}{kT}\right). \tag{13}$$

Equation (13) assures that the level populations obey the Boltzmann distribution when the radiative transitions are negligible compared to the collisional transitions.

Since data of the collisional transition rates are given for only low temperatures (e.g., $\leq 30$ K in Monteiro 1985), we extrapolate the deexcitation rates for higher temperatures proportionally to $\sqrt{T}$ assuming that the cross section would not vary drastically with temperature in the transition rate, $\langle \sigma v \rangle$. Although this assumption is rather crude, it would cause no significant error in the level populations because the density is high enough for the population to achieve the Boltzmann distribution (or LTE) wherever the temperature exceeds 30 K in our present problems.

TABLE 1

MOLECULAR PARAMETERS 1

| Molecule | $B$[a] | $\mu_d$[b] | $X$[c] | $N$[d] |
|---|---|---|---|---|
| CS..... | 24.4956 | 1.958 | $4 \times 10^{-9}$ | 10 |
| $HCO^+$..... | 44.5929 | 3.3 | $1 \times 10^{-8}$ | 6 |
| $H^{13}CO^+$..... | 43.3772 | 3.3 | $1 \times 10^{-10}$ | 6 |

[a] Rotation constant in GHz.
[b] Electric dipole moment in debye.
[c] Fractional abundance relative to $H_2$.
[d] Levels of $J = 0$–$N$ are considered in calculations.

### 3.2. *Results*

Figure 1 shows molecular line profiles of $HCO^+$ and $H^{13}CO^+$ ($J = 3$–2 and 4–3). Four stages of the main accretion phase of the evolution were chosen: at the initial stage (labeled "1"), just after the first core is formed ("6"), at the early stage ("12"), and at the late stage ("13"). Curve 12 corresponds to the class 0 or early class I phase and curve 13 to more evolved stages. Refer to Table 3, which is taken

TABLE 2

MOLECULAR PARAMETERS 2

| Molecule | Transition | Frequency (GHz) | Resolution[a] (arcsec) | Resolution[b] (AU) |
|---|---|---|---|---|
| CS..... | $J = 1$–0 | 48.99115 | 60 | 9000 |
| | $J = 2$–1 | 97.98230 | 60 | 9000 |
| | $J = 3$–2 | 146.97345 | 60 | 9000 |
| | $J = 4$–3 | 195.96460 | 60 | 9000 |
| $HCO^+$..... | $J = 1$–0 | 89.1858 | 69 | 10350 |
| | $J = 2$–1 | 178.3716 | 35 | 5250 |
| | $J = 3$–2 | 267.5574 | 23 | 3450 |
| | $J = 4$–3 | 356.7432 | 17 | 2550 |
| $H^{13}CO^+$..... | $J = 1$–0 | 86.7544 | 71 | 10650 |
| | $J = 2$–1 | 173.5088 | 36 | 5400 |
| | $J = 3$–2 | 260.2632 | 24 | 3600 |
| | $J = 4$–3 | 347.0176 | 19 | 2850 |

[a] A 10 m telescope is assumed except for CS lines, where a constant resolution is given for comparison with Zhou 1992.
[b] The object is assumed to be at a distance of 150 pc from an observer, i.e., $1'' = 150$ AU.

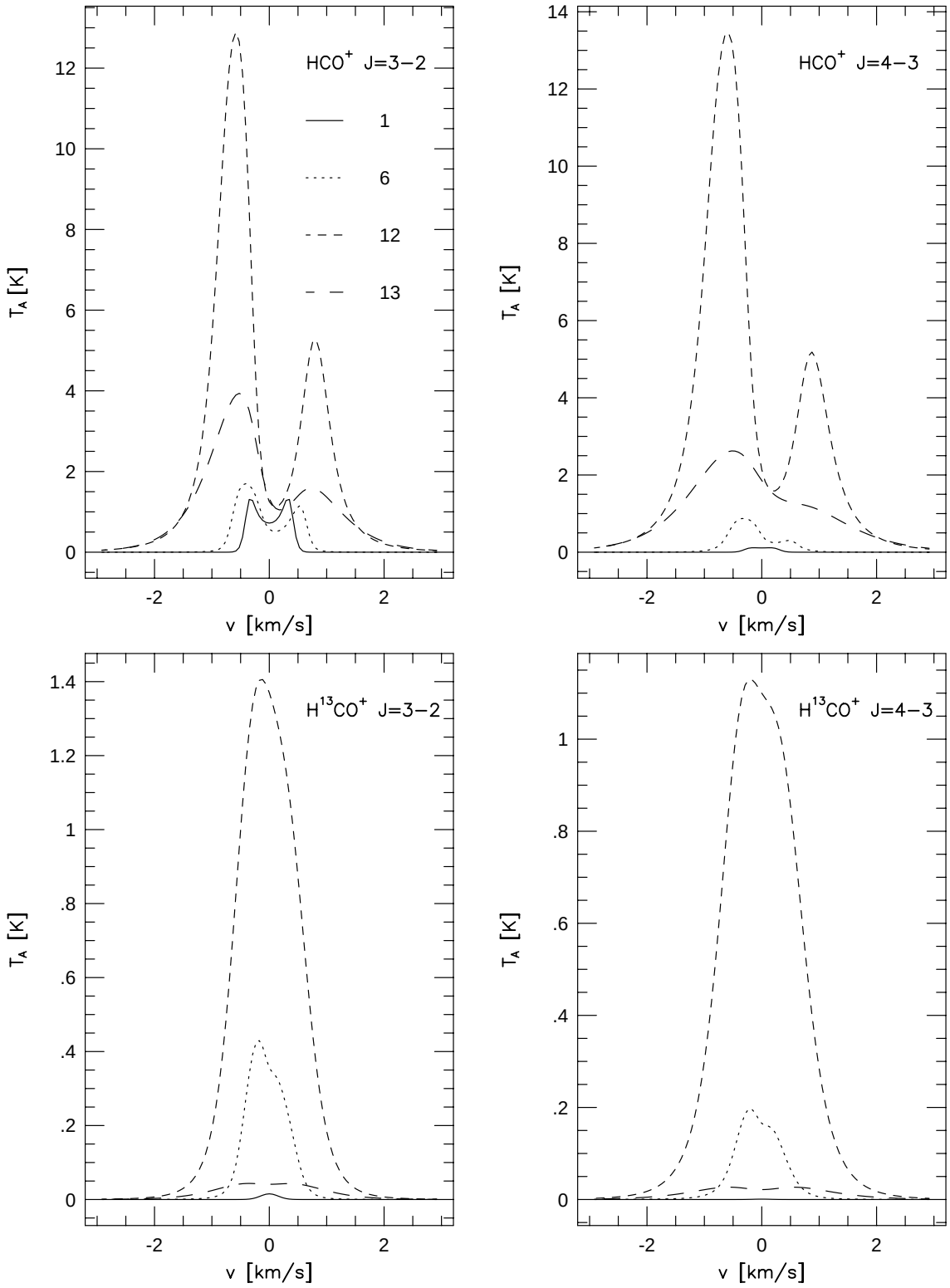


FIG. 1.—Computational results of spectral line synthesis for $HCO^+$ and $H^{13}CO^+$ ($J = 3$–2 and 4–3) are shown. Line profiles are given for the initial condition ("1"), just after the first core is formed ("6"), the early stage ("12"), and the late stage ("13") of the main accretion phase. Refer to Table 3 for label numbers.

from Masunaga & Inutsuka (2000), for the elapsed time corresponding to each label number.

While the kinetic temperature is almost constant throughout the cloud core at the initial stage, the excitation temperature, $T_{ex}$, decreases with radius near the outer boundary (Fig. 2, *upper left panel*) because the initial density is too low to collisionally excite levels against the deexcitations by spontaneous emission. A static cloud core with outwardly decreasing $T_{ex}$ produces a symmetric double-peaked profile for an optically thick line, which appears in $HCO^+$ $J = 3$–2 at the initial stage. For the other lines shown in Figure 1 the initial profiles are resolved out.

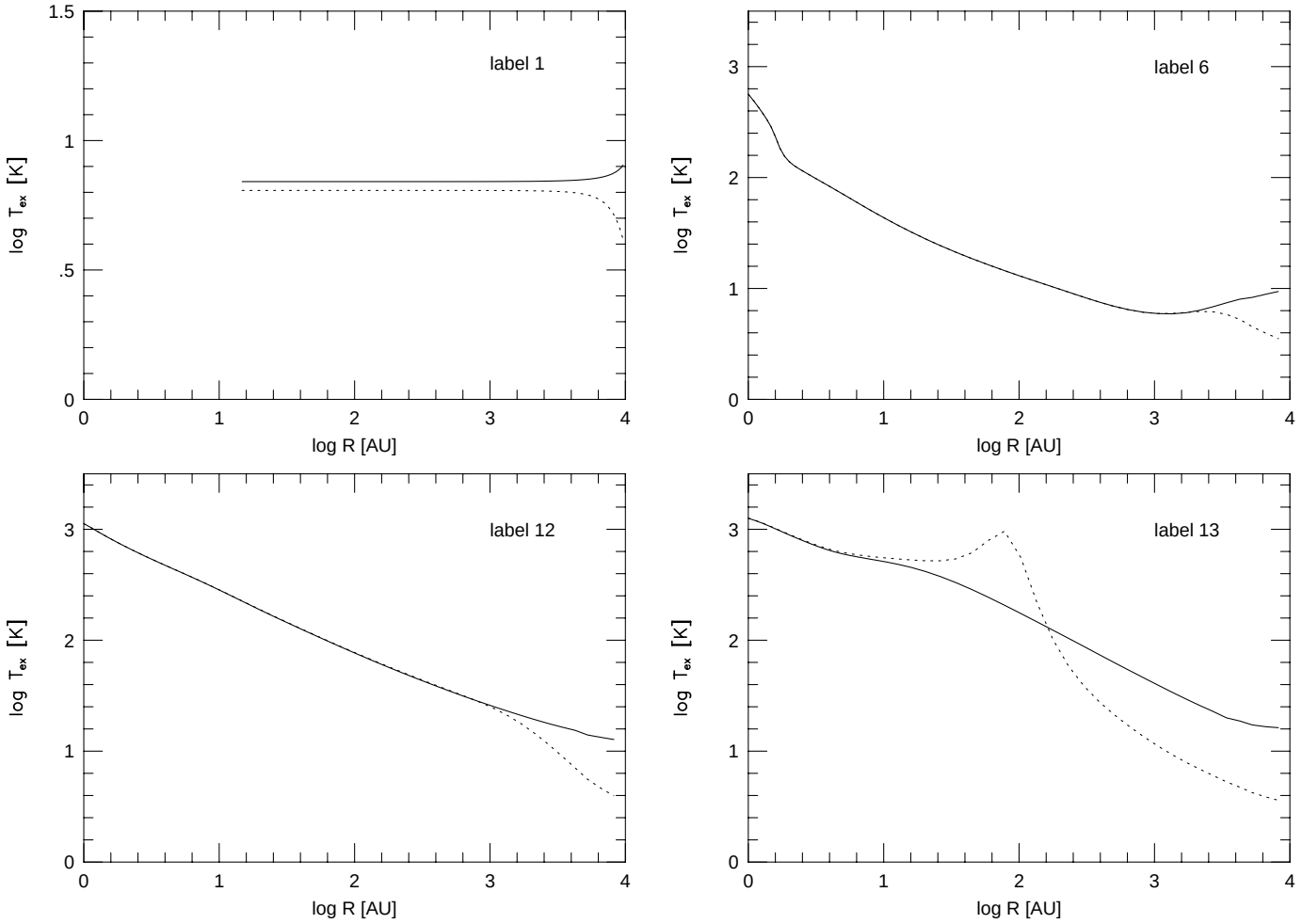


FIG. 2.—Excitation temperature, $T_{ex}$, of $HCO^+(J = 3–2)$ (*dotted lines*) as a function of radius as well as the kinetic temperature (*solid lines*), or equally, $T_{ex}$ under the LTE approximation. Each panel corresponds to each of the four evolutionary stages indicated by the label numbers shown.

TABLE 3

ELAPSED TIMES[a]

| Label | $t-t_0$[b] (yr) |
|---|---|
| 1 ..... | $-1.7522 \times 10^5$ |
| 6 ..... | $-1.2656 \times 10^0$ |
| 12 ..... | $2.2958 \times 10^4$ |
| 13 ..... | $1.3788 \times 10^5$ |

[a] Taken from Masunaga & Inutsuka 2000.

[b] The offset of time, $t_0 \equiv 1.7526 \times 10^5$ yr, represents the instance when the second collapse begins (or the instance when a protostar is born).

As the evolution proceeds, double-peaked profiles with a blue asymmetry appear in optically thick lines ($HCO^+$), as also found by past studies (Zhou 1992; Zhou et al. 1993; Walker, Narayanan, & Boss 1994). Portraying the mechanism of the spectral line formation of these asymmetric features according to the usual manner, Figure 3 illustrates the velocity field of the projected velocity to the line of sight just after the first core is formed (curve 6) within the 30 AU × 30 AU region in the center. The qualitative nature of the velocity field is similar at the more evolved stages. Examination of the figure reveals that there are two intersections by the

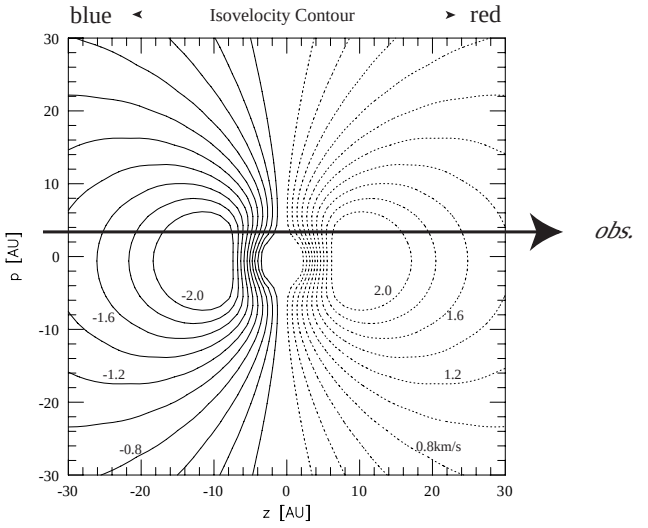


FIG. 3.—The isovelocity contour lines of the projected velocity to the line of sight just after the first core is formed (curve 6) within the 30 AU × 30 AU region in the center. The qualitative nature of the velocity field is similar at the more evolved stages. The solid lines correspond to the blueshifted components, and the dotted lines correspond to the redshifted components. The velocity interval between the adjacent contour lines is 0.2 km $s^{-1}$, and the highest level is 2.0 km $s^{-1}$.

line of sight for each contour curve for all redshifted and blueshifted velocities. The first intersection to an observer occurs in the outer redshifted component, while the first blueshifted intersection occurs closer to the central object. Since the excitation temperature decreases with radius, the blue component in a spectrum should therefore be more intense than the red component, provided the observed molecular line is optically thick enough. Spectral profiles of an opaque line should have a deep absorption feature at the line center because the bulk of the gas remains cold and almost at rest near the edge of the cloud. This cold, low-velocity gas absorbs the radiation from the active region in the cloud center.

The moment just after the first core is formed, labeled "6," also corresponds to the instance just before the birth of a protostar (cf. Masunaga & Inutsuka 2000). As an observational counterpart, Onishi, Mizuno, & Fukui (1999) reported a protostellar condensation in Taurus that is very close to the moment of the formation of a protostellar core. The observed spectral profiles of $HCO^+$ $J = 3$–2, 4–3 and $H^{13}CO^+$ $J = 3$–2, 4–3 (Fig. 2 in Onishi et al. 1999) are quite similar to our calculated profiles labeled "6" in Figure 1.

The most intensive feature in Figure 1 is seen in an early stage of the main accretion phase, when the maximum value is achieved in the luminosity (Masunaga & Inutsuka 2000). At the end of the main accretion phase, the peak intensity decreases again because of the non-LTE effect (described below) and because of the depletion of material in the infalling envelope. On the other hand, line widths continue growing throughout the evolution. Wings extend to $v = \pm 2$ km s$^{-1}$ in the main accretion phase. Wing components survive even after the peak intensity is diminished, because the infall velocity becomes larger as the gravitational potential is deepened by the growth of the protostellar mass.

The optically thin lines ($H^{13}CO^+$) show single-peaked profiles with a slight blue asymmetry. The line width increases monotonically with time similarly to the optically thick lines (Table 4). An optically thin line is helpful to discriminate the infall signature from other possible interpretations of the double-peaked profiles in opaque lines. Cloud complexes that have two separate velocity components would also show a double-peaked line profile, but the double peaks should appear in both optically thick and thin lines in such a case. A set of double-peaked opaque lines and single-peaked transparent lines with a blue asymmetry is strong evidence for infall motions.

TABLE 4

VELOCITY WIDTHS

| MOLECULE | TRANSITION | $\Delta V$[a] (km s$^{-1}$) 1 | 6 | 12 | 13 |
|---|---|---|---|---|---|
| CS..... | $J = 1$–0 | 0.770 | 1.07 | 1.41 | 1.45 |
| | $J = 2$–1 | 0.911 | 1.23 | 1.77 | 2.01 |
| | $J = 3$–2 | 0.854 | 1.28 | 2.00 | 2.58 |
| | $J = 4$–3 | 0.707 | 1.30 | 2.23 | 3.38 |
| $HCO^+$ ..... | $J = 1$–0 | 0.645 | 0.885 | 1.22 | 1.22 |
| | $J = 2$–1 | 0.725 | 1.06 | 1.69 | 1.85 |
| | $J = 3$–2 | 0.672 | 1.06 | 1.93 | 2.27 |
| | $J = 4$–3 | 0.485 | 1.04 | 2.10 | 2.57 |
| $H^{13}CO^+$ ..... | $J = 1$–0 | 0.384 | 0.615 | 0.810 | 0.885 |
| | $J = 2$–1 | 0.382 | 0.704 | 1.03 | 1.44 |
| | $J = 3$–2 | 0.360 | 0.812 | 1.26 | 2.04 |
| | $J = 4$–3 | 0.358 | 1.027 | 1.53 | 2.54 |

[a] The velocity width, $\Delta V$, is defined by eq. (14). Refer to Table 3 for label numbers. See also Figs. 1 and 6.

In order to demonstrate the significance of non-LTE effects, we have also performed additional calculations assuming LTE (Fig. 4). As shown by Figure 1, the LTE peak intensities in the optically thin lines are largely overestimated at every stage throughout the evolution because the kinetic temperature, or the LTE temperature, is systematically higher than the actual excitation temperature in non-LTE calculations (Fig. 2). For optically thick lines, one can easily see that an LTE calculation fails to produce a shallower absorption dip in the line center, since LTE calculations cannot reproduce a rapid decrease with radius of $T_{ex}$ near the cloud edge as observed in the non-LTE results. Figure 2 also shows that the excitation temperature at the final stage exceeds the kinetic temperature where $1 \lesssim \log R(\mathrm{AU}) \lesssim 2$, where the infalling gas is directly irradiated by hot photons from the central region and thus the molecular energy levels are pumped up to higher states more frequently than expected by the Boltzmann distribution for the local kinetic temperature. In a significant fraction of the cloud core [$\log R(\mathrm{AU}) \gtrsim 2$], however, the excitation temperature falls below the kinetic temperature because of the attenuation of hot photons and lowered density due to the depletion of the material. These effects cause a substantial overestimation of the emissivity in LTE calculations compared to the true non-LTE case as well as for the optically thin lines. This also explains why the LTE peak intensity keeps growing with time even at the final stage (curve 13) for the optically thick line ($HCO^+$) in contrast to the non-LTE case (compare Fig. 4 with Fig. 1). In the optically thin lines, the LTE peak intensity decreases with time at the final stage (curve 13), where the depletion of the infalling material cancels the overestimation of $T_{ex}$. The line profile of $HCO^+$ (labeled "6") exhibits red asymmetry in Figure 4 because the kinetic temperature *increases* with radius near the cloud edge as a result of the heating by optical photons incident through the outer boundary (Masunaga & Inutsuka 2000).

We also present in Figure 5 spectral profiles convolved by an off-center Gaussian beam by 40″ (6000 AU). The line profiles are totally different from those convolved by the centered beam. The peak intensity is weak even at the most active phase (curve 12). The lines remain narrow throughout the evolution and wings never come out. These significant changes in the line properties indicate that the broadening of lines and the appearance of wings are produced in a confined (relatively high density) region near the center, and thus they are diluted away in an off-center beam. The blue asymmetry becomes weaker in an off-center beam for the $HCO^+$ $J = 3$–2 line, and it completely disappears from the other lines shown in Figure 5. In general, an off-center beam suppresses the infall signatures.

We define a line width, $\Delta V$, according to Zhou (1992) as follows:

$$\Delta V = 2[2 \ln 2(\langle V^2 \rangle - \langle V \rangle^2)]^{1/2} , \qquad (14)$$

where the angle bracket indicates an average, $\langle q \rangle \equiv \sum (qT_A)/\sum T_A$. A Gaussian line profile yields $\Delta V$ equal to FWHM by this definition. Table 4 tabulates $\Delta V$ for each line profile. Line widths increase monotonically with time for every transition, reflecting the increasing infall velocity.

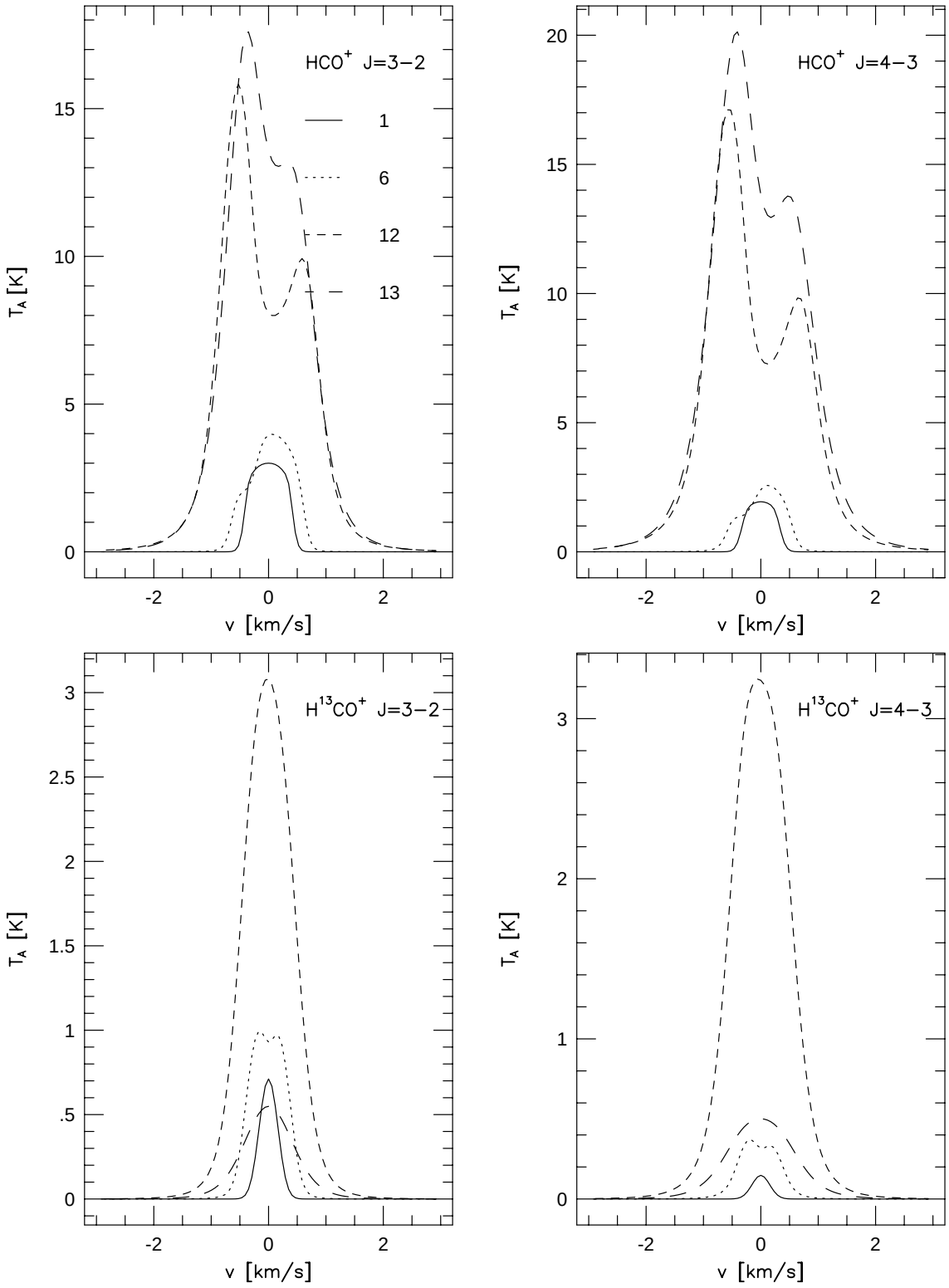


FIG. 4.—Spectral line profiles for $HCO^+$ and $H^{13}CO^+$ ($J = 3$–2 and 4–3) under the LTE approximation are shown. See also Fig. 1.

For comparison with the results by Zhou (1992), we perform spectral synthesis calculations for CS lines using the same parameters as adopted by Zhou for the fractional abundance ($X = 4 \times 10^{-9}$) and the resolution (60″ at 140 pc). We found that the largest line widths throughout the evolution are 1.45, 2.01, and 2.58 km $s^{-1}$ for CS $J = 1$–0, 2–1, and 3–2 lines, respectively, at the end of the main accretion phase. As the dynamical evolution resembles the LP model rather than the Shu model (Masunaga et al. 1998), our results should be compared with the "LP flow" in Zhou (1992). Zhou obtained $\Delta V = 4.03$, 4.24, and 4.43 km $s^{-1}$ for CS $J = 1$–0, 2–1, and 3–2, respectively, at a corresponding evolutionary stage ($t = 1.5 \times 10^5$ yr) for the "LP flow." The line widths obtained by Zhou are significantly

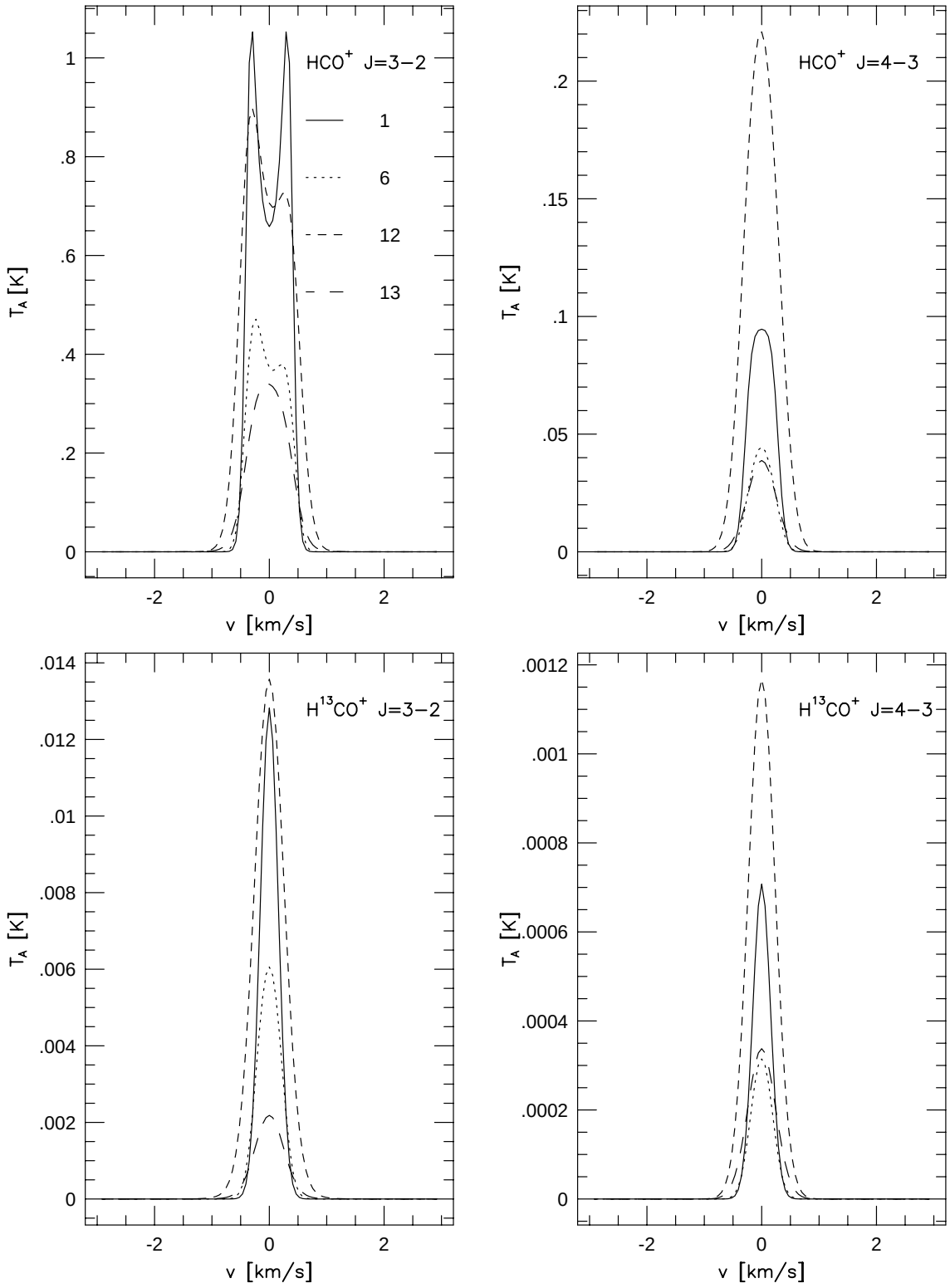


FIG. 5.—Spectral line profiles convolved by an off-center beam by 40″ for $HCO^+$ and $H^{13}CO^+$ ($J = 3$–2 and 4–3) are shown. See also Fig. 1.

larger than our results. Zhou excluded the LP flow because of the overestimation of the line width, but our results do not suffer from such unrealistically broad line profiles. Indeed, our results for CS line profiles (Fig. 6) are totally different from Zhou's "LP flow" profiles, which showed an extremely broad absorption at the line center. As predicted in § 1, the very large $\Delta V$ found by Zhou (1992) is due to a large value of the infall velocity ($3.3c_s$) at large radii in the "naive" LP model, while the velocity declines to zero near the outer boundary in a "realistic" LP model that we obtained, which yields acceptable values for $\Delta V$.

Another important result of our calculation is the existence of wings extending to $v = \pm 2$ km s$^{-1}$, in contrast to some past studies where wings could not be produced by

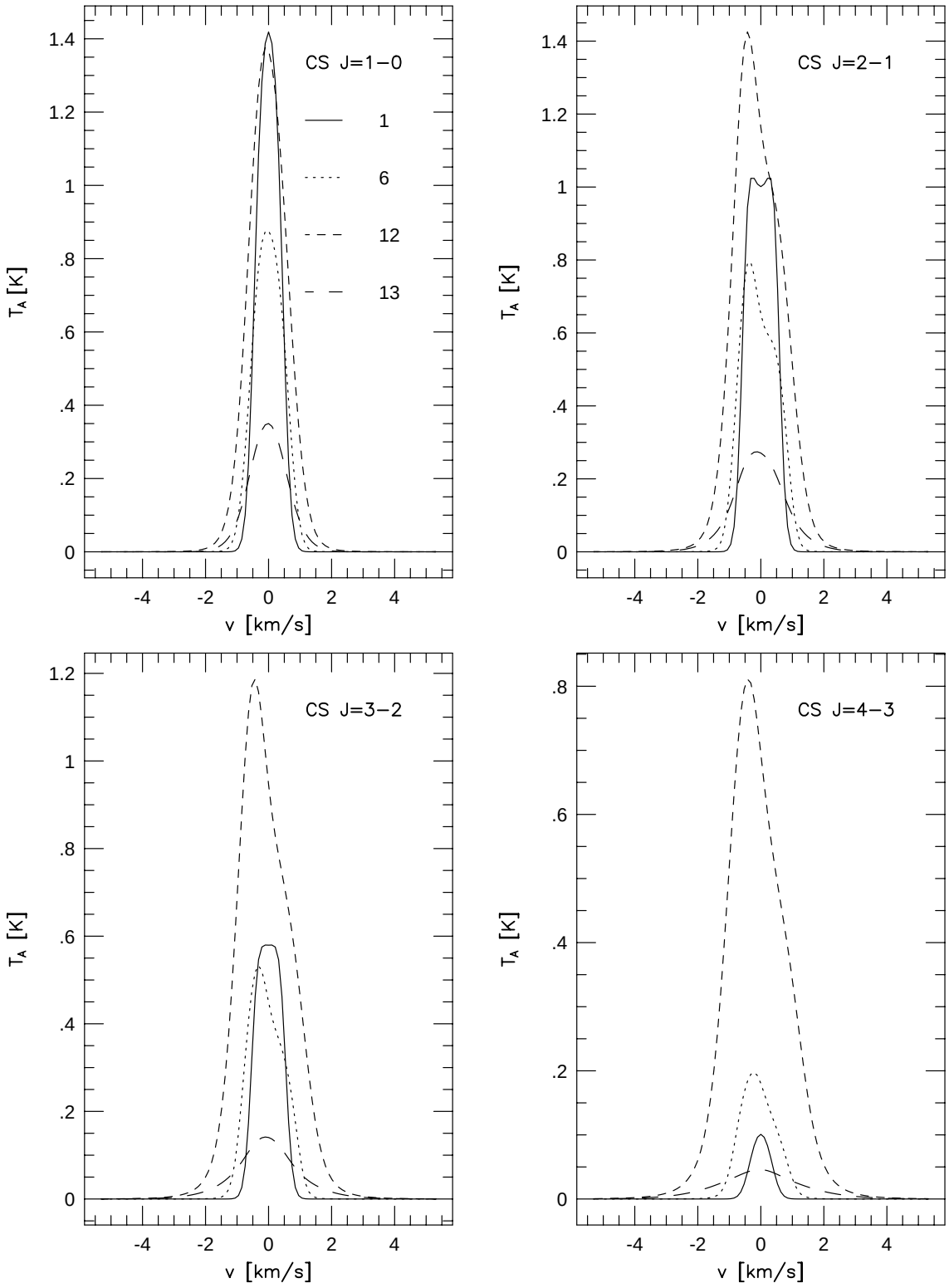


FIG. 6.—Computational results of the spectral line synthesis for CS ($J = 1$–0, 2–1, 3–2, and 4–3) are shown. Line profiles are given for the initial condition (" 1 "), just after the first core is formed (" 6 "), the early stage (" 12 "), and the late stage (" 13 ") of the main accretion phase. Refer to Table 3 for label numbers.

infall models (e.g., Gregersen et al. 1997). A main reason why these past calculations failed to reproduce wings in line spectra may be attributed to the use of the expansion-wave collapse solution obtained by Shu (1977). The expansion-wave collapse solution consists of an inner free-falling region and a surrounding hydrostatic envelope, where the latter gives no contribution to the high-velocity wing. Moreover, the expansion-wave collapse solution has the minimum mass accretion rate ($\dot{M} = 0.975 c_s^3/G$ at the origin) among the family of the isothermal self-similar solutions that include the singular origin. Hence, the growth rate of the central point mass (or a protostar) is so slow that the

gravitational potential grows only gradually, which is less efficient to produce the high-velocity wings.

Walker et al. (1986) obtained wings at $v \approx \pm 2$ km s$^{-1}$ assuming a collapse model resembling the expansion-wave collapse solution, which may imply that the expansion-wave collapse solution does not always fail to explain the presence of wings. However, Walker et al. (1986) modified the inner portion of the expansion-wave collapse solution to fit observations, and thus the density and velocity distributions are not treated self-consistently for $r < 10^{16}$ cm, where the wing emission is produced. Moreover, the peak intensities and the depth of the absorption dip show some disagreement between the model and the observation for even their best-fit model. While the simpler models used by earlier workers may be useful in obtaining a "first-order" understanding of conditions in a collapsing cloud core, a detailed analysis and quantitative prediction of line spectra require more realistic collapse models.

Our results do not exclude possible contamination of outflows in observed spectra. Since 87% of class 0 and I sources show evidence of driving an outflow (Mardones et al. 1997), the contamination would be inevitable. Although quantitative studies on the contamination of outflows require a reliable model for molecular outflows in the future, some qualitative or statistical methods are available to discriminate the signature of outflows from that of infalls in line spectra. In order to distinguish the contribution of infalls from that of outflows in line spectra of actual objects, intensity maps in different velocity ranges would be helpful. While both the blue and red intensities integrated along the line of sight would exhibit similar spatial distributions when the infall dominates the line formation, the blue and red wing intensities might be peaked on off-center positions in different directions in the map (Gregersen et al. 1997).

Rotation of the protostellar envelopes would also affect the line formation in actual protostellar objects. Intensity maps would be helpful again for separating the signature of rotation from that of infall in observed emissions. Walker et al. (1994) and Narayanan & Walker (1998) performed LTE radiative transfer calculations using nonspherical, three-dimensional models for spectral line synthesis. They reported that the "blue bulge" appears across the projected rotational axis in the intensity maps. The assumption of LTE, however, can cause errors in spectral line synthesis of protostellar objects, as shown in § 3.2 above. A non-LTE calculation for multidimensional models is required to obtain a more quantitative understanding of the effects that rotation has on spectral line formation in collapsing cloud cores.

## 4. SUMMARY

The results obtained in this paper are summarized as follows.

1. We have developed a spherically symmetric, numerical code for non-LTE line transfer problems and have applied it to protostar formation. Our formulation uses neither the LVG (or Sobolev) nor microturbulence approximations and is therefore applicable to arbitrary distributions for density, temperature, and velocity. For dynamical models, RHD calculations are used, where the density, temperature, and velocity distributions are obtained in a self-consistent manner.

2. We confirm that the computational results show double-peaked profiles with a stronger blue peak for optically thick molecular lines. Optically thin lines show single-peaked profiles with a slight blue asymmetry. These qualitative features are consistent with past studies.

3. The peak is most intensive at an early stage of the main accretion phase, which corresponds to the genuine class 0 phase (see Masunaga & Inutsuka 2000). While the peak intensity is lowered in later stages, line widths increase monotonically with time. The LTE approximation leads to qualitatively different trends from the true non-LTE results in spectral profiles. An off-center beam is found to suppress the infall signatures. Contrary to the remarks by Zhou (1992), we did not find an overestimation of line widths when the dynamical evolution resembles the LP model rather than the Shu model. Modest values of line widths are obtained under a realistic boundary condition.

4. The infall motion also produces wings extending to $v = \pm 2$ km s$^{-1}$ in line spectra. Wings could not be produced in some previous works where the expansion-wave collapse solution was adopted as the infall model. Our results show that the presence of wings in line spectra does not always mean the existence of outflows.

As a consequence of the present paper, we found that an RHD model reproduces typical features in line spectra of class 0 and I sources more naturally than the isothermal self-similar solutions. Simplified infall models, such as the isothermal similarity solutions adopted by previous authors, are not always suitable to the detailed modeling of line spectra.

The authors greatly appreciate the helpful comments of Yasuo Fukui and Toshikazu Onishi. The authors are also very grateful to the anonymous referee for instructive comments, which helped us polish the manuscript and led us to a better understanding of past investigations related to this study. The research of H. M. is supported by the Research Fellowships of the Japan Society for the Promotion of Science for Young Scientists.

## REFERENCES

Choi, M., Evans, N. J., II, Gregersen, E. M., & Wang, Y. 1995, ApJ, 448, 742
Green, S. 1975, ApJ, 201, 366
Green, S., & Chapman, S. 1978, ApJS, 37, 169
Gregersen, E. M., Evans, N. J., II, Zhou, S., & Choi, M. 1997, ApJ, 484, 256
Hunter, C. 1977, ApJ, 218, 834
Larson, R. B. 1969, MNRAS, 145, 271
Leung, C. M., & Brown, R. L. 1977, ApJ, 214, L73
Mardones, D., Myers, P. C., Tafalla, M., Wilner, D. J., Bachiller, R., & Garay, G. 1997, ApJ, 489, 719
Masunaga, H. 1999, Ph.D. thesis, Univ. Tokyo
Masunaga, H., & Inutsuka, S. 2000, ApJ, 531, 350
Masunaga, H., Miyama, S. M., & Inutsuka, S. 1998, ApJ, 495, 346
Monteiro, T. S. 1985, MNRAS, 214, 419
Narayanan, G., & Walker, C. K. 1998, ApJ, 508, 780
Onishi, T., Mizuno, A., & Fukui, Y. 1999, PASJ, 51, 257
Penston, M. V. 1969, MNRAS, 144, 425
Shu, F. H. 1977, ApJ, 214, 488
Snell, R. L., & Loren, R. B. 1977, ApJ, 211, 122
Walker, C. K., Lada, C. J., Young, E. T., Maloney, P. R., & Wilking, B. A. 1986, ApJ, 309, L47
Walker, C. K., Narayanan, G., & Boss, A. P. 1994, ApJ, 431, 767
Zhou, S. 1992, ApJ, 394, 204
Zhou, S., Evans, N. J., II, Kömpe, C., & Walmsley, C. M. 1993, ApJ, 404, 232